Hierarchical Hybridization in Plasmonic Honeycomb Lattices

Ran Li^{1,}†, Marc R. Bourgeois^{3,}†, Charles Cherqui^{3,}†, Jun Guan², Danqing Wang², Jingtian Hu¹, Richard D. Schaller³, George C. Schatz^{*, 3} and Teri W. Odom^{*, 1, 3}

Abstract

This paper reports hierarchical hybridization as a mode-mixing scheme to account for the unique optical properties of non-Bravais lattices of plasmonic nanoparticles (NPs). The formation of surface lattice resonances (SLRs) mediated by localized surface plasmons (LSPs) of different multipolar orders, e.g. dipole and quadrupole, can result in asymmetric electric nearfield distributions surrounding the NPs. This asymmetry is because of LSP hybridization at the individual NP level from LSPs of different multipole order and at the unit-cell level (NP dimer) from LSPs of the same multipole order. Fabricated honeycomb lattices of silver NPs exhibit ultra-sharp SLRs at the Γ point that can also facilitate nanolasing. Modeling of the stimulated emission process revealed that the multipolar component of the lattice plasmon mode was responsible for feedback for lasing. By leveraging multipolar LSP responses from aluminum NPs lattices, we achieved two distinct Γ point band-edge modes from a single honeycomb lattice. This work highlights how multipolar LSP coupling in plasmonic lattices with a non-Bravais symmetry have important implications for the design of SLRs and their associated plasmonic near-field distributions. These relatively unexplored degrees of freedom can decrease both ohmic and radiative losses in nanoscale systems and enable SLRs to build unanticipated connections among photonics and nanochemistry.

¹Department of Materials Science and Engineering

²Graduate Program in Applied Physics

³Department of Chemistry, Northwestern University, Evanston, Illinois, 60208, USA

Keywords: dipole-quadrupole coupling, surface lattice resonances, metal nanoparticles, lattice plasmons, plasmonic nanolasing, honeycomb lattice

Two-dimensional (2D) materials with honeycomb lattice symmetry exhibit unusual conductive and optical properties because of degeneracies at the high-symmetry points in the electronic band structure. In solids, band structure emerges from the interplay between global lattice symmetry and interactions between atomic wavefunctions at each site. In 2D lattices of plasmonic nanoparticles (NPs), an analogous photonic band structure can result, where atomic wavefunctions are replaced by surface-bound electron oscillations known as localized surface plasmons (LSPs) or LSP wavefunctions. By exploiting the intrinsic size-and-composition tunability of the LSP wavefunctions, NP units offer a programmable basis set that does not exist in electronic systems. For example, as the distance between NPs becomes commensurate with an integer multiple of the wavelength of incident light, collective lattice modes emerge that can be rationally tuned based on the diffractive character of the 2D array as well as the induced charge distribution of LSPs. These lattice plasmons, also called surface lattice resonances (SLRs), are characterized by an energy dispersion relation $E(\mathbf{k}_{\parallel})$, where \mathbf{k}_{\parallel} is the in-plane wave vector. In 12

The photonic band structure of SLRs can be constructed directly from transmission spectra and indirectly from the back-focal plane of a microscope or spectroscopic ellipsometry. ¹²⁻¹⁹ Early work reported that there were no major differences among the linear optical properties of square, rectangular, hexagonal, and honeycomb lattices at the Γ point ($|\mathbf{k}_{\parallel}| = 0$) based on dipole (D) interactions between units. ²⁰ An analysis of the mode symmetries and far-field polarization properties of the K-point SLRs supported by a plasmonic honeycomb lattice were also recently

reported.²¹ Reports that captured SLR dispersion characteristics showed clear differences due to lattice symmetry, but since the data was analyzed only according to the free-photon dispersion relation, effects of scattering from NPs on the resulting band structure were not considered.¹⁵ The relationship between lattice symmetry and contributions of higher-order LSPs to SLRs has just started to receive attention. Quadrupolar (Q) coupling in plasmonic NP lattices show characteristics from out-of-plane Q-Q interactions that are similar to those from D-D coupling.²¹⁻²⁴ Although SLRs from in-plane Q-Q coupling have been observed in *finite* square lattices,²¹ these modes are optically dark in the infinite lattice limit. Also, the focus on SLRs in Bravais lattices has been on modes mediated by LSPs of the same multipolar order because SLR modes of mixed D-Q character are not accessible at the Γ point in systems of such symmetries.²² In the case of non-Bravais lattices, where D-Q coupling is allowed at the Γ point, only far-field observables have been reported, with near-field signatures missing.^{15, 21}

Recent interest in the band structure of SLRs has been motivated in part by the emergence of topological photonics in dielectric NP arrays. The low losses associated with dielectric NPs allow for defect-tolerant unidirectional propagating edge states, ^{25, 26} and topological states in plasmonic systems have been considered. ^{23, 27, 28} However, topological effects are challenging to realize in metal systems because of radiative and ohmic losses. SLRs provide a potential strategy to explore topology-based phenomena because they can mitigate losses associated with plasmonic NPs. ²⁹ By exploring non-Bravais lattice symmetries and complex wavefunction hybridization at the unit-cell level, we can test how lattice symmetry and LSP wavefunction bases can be applied to plasmonic topological effects. ³⁰

Here we show that honeycomb plasmonic lattices can produce SLRs from the hybridization of same-order LSPs between lattice sites and hybridization of different-order LSPs at the same

lattice site. This mode-mixing scheme—hierarchical hybridization—is a result of the non-Bravais nature of the honeycomb lattice combined with the available LSP wavefunction basis of plasmonic NPs. Hybrid SLRs exhibit asymmetric surface-charge distributions on the NP surfaces that dominate the near-field, and whose effects can be visualized by plasmonic lasing with silver NP lattices. We extended and leveraged the LSP wavefunction basis to create a single lattice that could support two distinct band-edge SLRs that were spectrally separated by ca. 300 nm in aluminum NP lattices. This work highlights a distinct feature of plasmonic NP lattices that enables an unexpected class of hybridization not possible in other nanophotonics systems.

Figure 1a indicates how the honeycomb lattice can be described as a hexagonal lattice with a two-unit basis or a superposition of two identical but non-equivalent hexagonal sublattices L₁ (red) and L₂ (blue). L₁ and L₂ are related by an inversion operation and are characterized by two length scales: (1) the magnitude of the basis vectors of each hexagonal sublattice a; and (2) the distance between adjacent NPs in the honeycomb lattice $a_0 = a/\sqrt{3}$. Figure 1b shows a honeycomb lattice ($a_0 = 400$ nm) made of Ag NPs (d = 110 nm diameter) fabricated by soft nanolithography.³¹ The NP dimensions were chosen to optimize the SLR mode at the Γ point

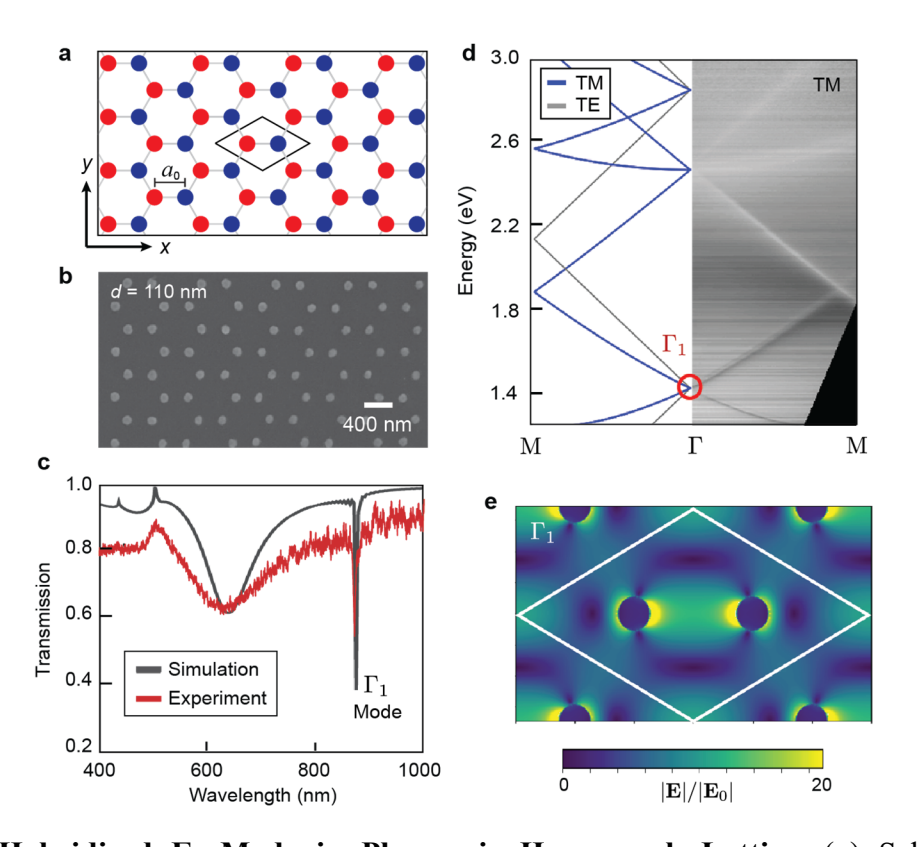


Figure 1. Hybridized Γ_1 Mode in Plasmonic Honeycomb Lattice. (a) Scheme of a honeycomb lattice with two NPs per unit cell (outlined). Red and blue sites belong to hexagonal sub-lattices L₁ and L₂, respectively. (b) SEM image of fabricated honeycomb lattice ($a_0 = 400$ nm) of Ag NPs with d = 110 nm and h = 50 nm. (c) Calculated and measured transmission spectra of lattice in (b) for x-polarized plane waves at the Γ point showing strong SLR Γ₁. (d) Calculated (left) and measured (right) dispersion diagram (angle-dependent transmission of TM polarized plane wave) for the lattice in (b) along the Γ – M path through the Brillouin zone. (e) Calculated electric field magnitude within the xy plane of honeycomb unit cell excited at $\lambda_{\Gamma 1}$ showing asymmetric spatial distributions characteristic of multipolar LSP superposition.

(873 nm or 1.42 eV) (**Figure 1c**) to have a quality factor \approx 170 and a FWHM \approx 5 nm. The broad feature near 625 nm (2.0 eV) is the single-NP LSP response. The transmission spectrum calculated using the finite-difference time-domain (FDTD) method²⁴ using periodic boundary conditions is accurate when fabricated samples are patterned over large enough areas (\sim cm²) to be considered infinite.^{21,32}

The dispersion diagram of the fabricated Ag NP honeycomb lattice was mapped along the Γ -M direction through the Brillouin zone by measuring transmission spectra of x-polarized TM plane waves (polarization vector parallel to the plane of incidence) as a function of incident angle (**Figure 1d**, right). The experimental dispersion diagram is similar to the calculated TM-polarized photonic cavity dispersion relation¹⁵ except near the high-symmetry Γ_1 (1.42 eV, 873 nm) and M (1.87 eV, 664 nm) points, where deviations emerge from the formation of band-edge states as a result of NP scattering (**Figure 1d**, left). The narrow spectral feature in the normal-incident transmission spectrum (Figure 1c) can be assigned as a Γ_1 point SLR with associated electric near-field distribution (**Figure 1e**). Because honeycomb (non-Bravais) lattices and hexagonal (Bravais) sublattices are characterized by the same reciprocal lattice, both geometries exhibit qualitatively similar Γ point transmission spectra^{15, 20} (**Figure S1**).

We identified the multipolar LSP contributions to the Γ_1 SLR mode in honeycomb lattices by examining the LSP modes supported by both one- and two-particle hexagonal and honeycomb unit cells. **Figure 2a** shows calculated extinction cross sections of a h = 50 nm and d = 110 nm Ag NP (single-particle unit cell) in a hexagonal sublattice under two excitation conditions. When the x-polarized incident plane wave propagates along the z-axis (red trace), a strong and broad LSP mode (D_{\parallel}) is excited near 2 eV (620 nm) as well as a weaker mode (Q_{\perp}) just above 3 eV (413 nm). A plane wave propagating along the y-axis and polarized along the x-axis (blue trace)

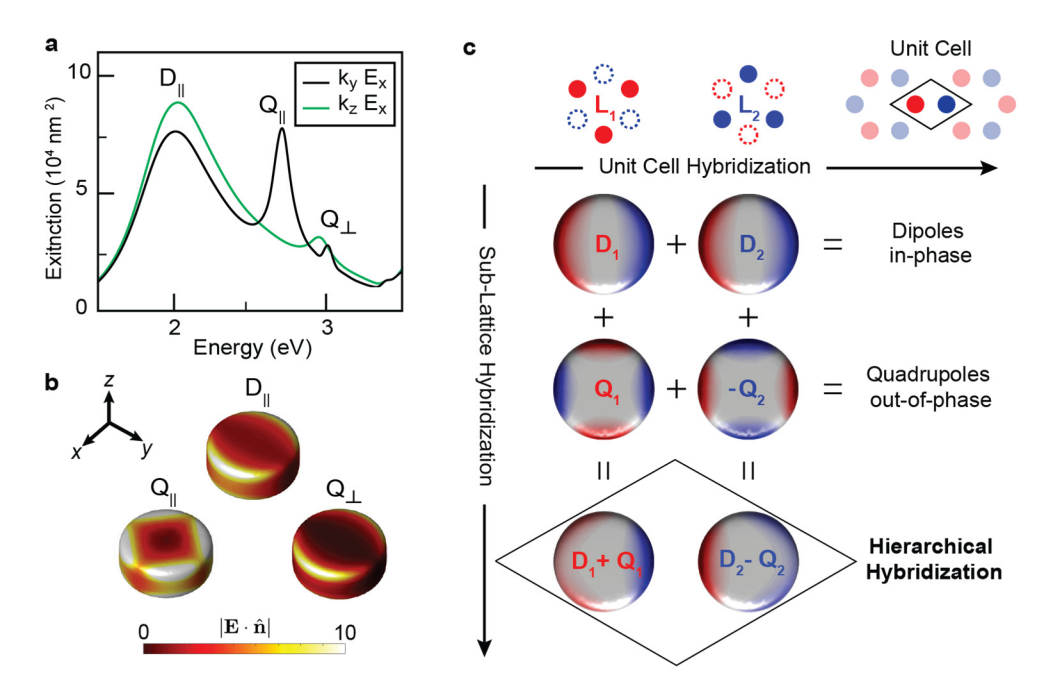


Figure 2. Hierarchical Hybridization at Γ_1 Resonance. (a) Calculated extinction spectra of isolated Ag disks (d = 110 nm and h = 50 nm) excited by plane waves with incident wave vector \mathbf{k} parallel (black) and perpendicular (green) to the disk symmetry axis. The dipole mode D_{\parallel} is excited in both cases, while the in-plane quadrupole Q_{\parallel} is not excited with \mathbf{k} directed along the z-axis. Note that the mode near 3.0 eV under k_y , E_x plane wave excitation is the electric octupole, but is not relevant to the current discussion and is not considered in the analysis. (b) Calculated electric fields associated with D_{\parallel} and Q_{\parallel} modes of the isolated disk projected onto the surface normal $\hat{\mathbf{n}}$ highlighting different near-field spatial distributions. (c) Hierarchical hybridization scheme showing the Γ_1 mode of the honeycomb lattice involves D-Q mixing on both sub-lattice (vertical) and unit cell (horizontal) levels. Red and blue colors correspond to positive and negative induced surface charges, respectively.

can also excite the D_{\parallel} mode along with a second resonance (Q_{\parallel}) near 2.72 eV (460 nm). Calculated electric fields at the energies of the D_{\parallel} and Q_{\parallel} modes near the NP surface enable a multipolar order to be assigned based on nodal structure (**Figure 2b**). The near-field distribution of the D_{\parallel} mode exhibits a single yz nodal plane characteristic of the in-plane electric dipole $D_{\parallel} \equiv p_x \hat{x}$ mode. The Q_{\parallel} mode is characterized by a set of xz and yz nodal planes and can be assigned as an in-plane quadrupole LSP mode. The Q_{\perp} mode is the out-of-plane quadrupole with yz and xy nodal planes. Interestingly, the electric near-field distribution around NPs at the Γ_1 SLR mode of

a hexagonal lattice (Figure S1) matches that of the D_{\parallel} mode (Figure 2b). This observation indicates that the Γ_{l} SLR mode of a hexagonal lattice is from hybridization between the D_{\parallel} LSPs with the Bragg mode of the lattice.

Surface charge distributions corresponding to eigenmodes of an isolated honeycomb lattice unit cell (i.e., a NP dimer) were calculated using the boundary element method (BEM) by solving for the roots of the determinant of the BEM matrix³³ (**Figure 2c**, first and second rows). The top row depicts in-phase coupling of D_{\parallel} LSP modes on L_1 and L_2 (labeled D_1 and D_2), and the second row depicts out-of-phase coupling of Q_{\parallel} (labeled Q_1 and Q_2) LSPs on the two sublattices. Other dimer modes, such as in-phase Q_{\parallel} and the out-of-phase D_{\parallel} modes are not considered since they are not observed in the near-field distribution (Figure 1e). Due to the relatively large NP-NP separation ($a_0 = 400$ nm), the energies of the dimer modes are nearly degenerate with the D_{\parallel} and Q_{\parallel} modes of an isolated Ag NP (**Figure S2**). In contrast to a hexagonal lattice, the honeycomb lattice supports a linear combination of the in-phase D_{\parallel} and out-of-phase Q_{\parallel} hybridized LSPs, which accounts for the near-field distribution in the FDTD simulations (Figure 1e).

Strikingly, the hybridization scheme of plasmonic honeycomb NP lattices is distinct (Figure 2c) and has no analogue in either electronic or dielectric (photonic) systems. Besides hybridization across the unit cell of a non-Bravais lattice, LSP wavefunctions of a single site can self-hybridize *via* the additional photon degree of freedom from the Bragg mode. This type of multipolar mode-mixing on a single NP (self-hybridization) has been observed for cubic metal NPs on a dielectric substrate, where the coupling between in-plane D and out-of-plane Q LSP modes is mediated by the substrate.^{34, 35} This effect can be suppressed, however, if the dipole and quadrupole LSP modes do not spectrally overlap. Plasmonic NP lattices are not constrained in

this way since the single- NP LSPs are coupled *via* the Bragg lattice modes. In the case of the Γ_1 SLR in the honeycomb lattice, the strong electromagnetic response of the multipolar LSPs and the non-Bravais character of the lattice allow the D_{\parallel} and Q_{\parallel} modes hybridized with the Bragg mode to become effectively degenerate on sublattices L_1 and L_2 . When the two hexagonal sublattices are combined to form a honeycomb lattice, hybridization occurs at both the single particle and unit-cell level—hence, hierarchical hybridization (Figure 2c).

With a detailed understanding of mechanism of the asymmetric near-fields of the hybrid SLRs, we used plasmon lasing as a diagnostic tool to examine this Γ point mode further. We placed a droplet of IR-140-DMSO solution (0.5 mM) on a 2D Ag NP lattice (same dimensions as in Figure 1) on a silica substrate and pumped the dye with a TM-polarized 800-nm fs-pulsed laser (Methods). The light emitted normal to the surface had a very narrow lasing peak (FWHM ≈ 0.2 nm) centered at 866 nm, close to the Γ_1 resonance (**Figure 3a**). Power-dependent input-output profiles showed a nonlinear increase in lasing intensity above threshold (~ 0.21 mJ/cm²),

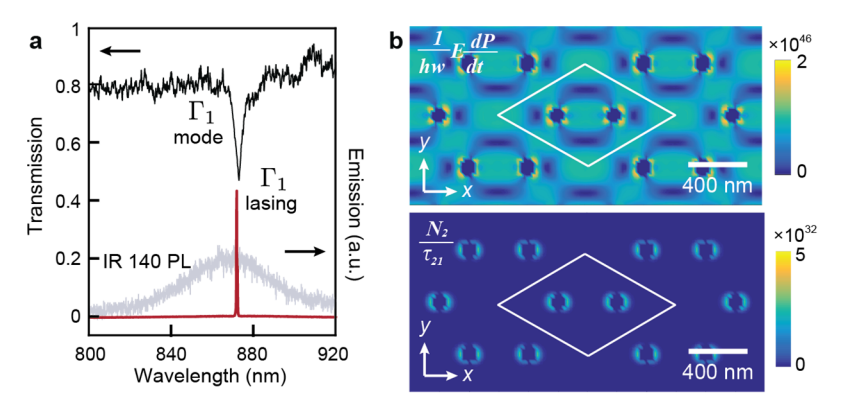


Figure 3. Dipole – Quadrupole Coupling Supports Lasing at Γ_1 Mode. (a) Lattice mode (black) spectrally overlapped with PL of IR 140 dye solution (light blue). The lasing emission spectrum (red) exhibits characteristic linewidth narrowing close to the Γ_1 mode of the lattice. (b) Calculated spatial distribution maps of the stimulated $(\frac{1}{\hbar w_a} E \frac{dP_a}{dt})$ and spontaneous (N_2/τ_{21}) emission rates when lasing occurred in units of s⁻¹·m⁻³. The stimulated emission spatial distribution matches that of the Q mode in Figure 2b.

and angle-resolved emission measurements indicate that the lasing emission was from the bandedge Γ_1 mode at $|\mathbf{k}_{\parallel}| = 0$ (**Figure S3**). We used our semi-quantum four-level, one-electron model of organic gain medium coupled to FDTD calculations to simulate lasing action.^{32, 36, 37} These calculations confirmed that the lasing occurred at the same wavelength as the Γ_1 resonance (**Figure S4**). The lasing emission supported by the Γ_1 SLR mode was at a slightly shorter wavelength compared to that of the Γ_1 SLR mode (Figure 1c) because of refractive index changes at high pump fluences or the optical pulling effect.^{24, 38} In contrast to plasmonic systems that have stimulated emission rate $(\frac{1}{hw_a}E^{dPa}_{dt})$ maps and spontaneous emission rate (N_2/τ_{21}) maps dominated by D-D or Q-Q coupled SLRs,^{24, 37, 39} lasing from the honeycomb lattices showed an asymmetric distribution of the stimulated emission rate because of hierarchical hybridization. Notably, different from the stimulated emission rate map, the spatial distribution of the spontaneous emission rate resembles that of a dipole LSP field (**Figure 3b**).

When the particle height is small (< 50 nm), the out-of-plane quadrupole degrees of freedom are not prominent in SLR excitations; however, these multipolar modes can be used to produce additional SLR modes²⁴ as NP height increases. To explore whether a single structure can support multiple high-quality SLRs over the visible to near-infrared wavelength range,^{40, 41} we fabricated Al NP honeycomb lattices with increased height (d = 110 nm, h = 100 nm, $a_0 = 400$ nm) on silica substrates with a DMSO superstrate for index matching. In addition to a sharp Γ_1 resonance ($\Gamma_1 = 873$ nm, FWHM ≈ 9 nm), a second sharp resonance appeared at higher energy that we label Γ_2 ($\Gamma_2 = 506$ nm, FWHM ≈ 5 nm) since this resonance is also observed at 0° incident angle (**Figure 4a**). At the Γ_2 resonance, the calculated surface charge distribution and the electric field ($|\mathbf{E}|^2/|\mathbf{E}_0|^2$) are localized to the upper and lower NP surfaces with xy and yz nodal planes for x-polarized light. The phase within the top- and bottom-halves of each NP are out-of-

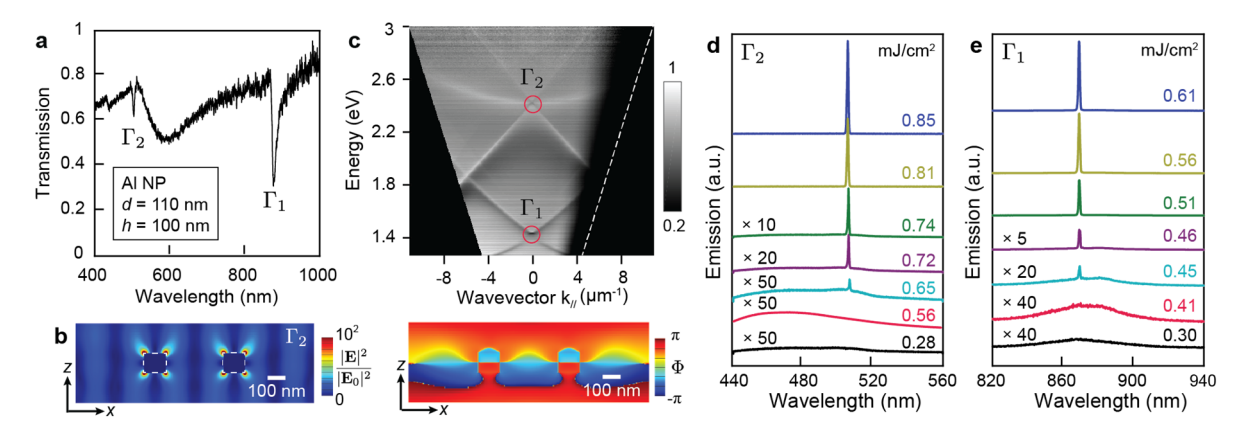


Figure 4. Lasing Supported by Two Distinct Band Edge States. (a) Measured transmission spectrum of Al NP (d = 110 nm, h = 100 nm) honeycomb lattice showing simultaneously optimized Γ_1 and Γ_2 modes. (b) Calculated electric field magnitude normalized by magnitude of incoming field ($|\mathbf{E}|^2/|\mathbf{E}_0|^2$) and phase profile of the Γ_2 mode. Scale bars are 100 nm. (c) Dispersion diagram of Al NP array under TM polarization. (d) Measured Γ_2 emission spectra with increasing pump power for Al NP array (LDS 473 dye concentration 20 mM). (e) Measured Γ_1 emission spectra with increasing pump power for Al NP array (IR-140 dye concentration 0.5 mM). The input-output curves can be found in Figure S5.

phase by π (**Figures 4b, S6**). These characteristics confirm that the Γ_2 mode is correlated with an out-of-plane quadrupole LSP, which in earlier work was labeled as a hybrid out-of-plane quadrupole (Q_⊥) lattice plasmon resonance because of the *superposition* of Q_⊥ with an overlapping dipolar LSP.²⁴ Therefore, the sharp Γ_2 resonance is from the stronger Q_⊥ LSP coupled to the (1, -1) Bragg mode with only minor overlap of the dipole LSP coupled to the (1, -1) Bragg mode (**Figure S7**). Note that this superposition is different from the explicit mode-mixing of hierarchical hybridization. The dispersion diagram of the fabricated Al NP lattice was experimentally mapped along Γ-M using TM-polarized light and showed two band-edge states at Γ_1 and Γ_2 points (**Figure 4c**).

Multiple lasing peaks were previously demonstrated from a NP superlattice composed of microscale arrays of finite-lattice patches.³² In contrast, by controlling the sub-wavelength lattice structure *via* unit cell design, we can access two different SLR modes that can support lasing

with a wavelength separation of ~ 300 nm using different organic gain. With LDS 473-DMSO (20 mM) pumped by a 400-nm fs-pulsed laser, the PL centered at 475 nm overlapped with the Γ_2 mode. A narrow lasing peak (FWHM ≈ 0.3 nm) at 505 nm was observed normal to the lattice plane (**Figure 4d**). The light-light curve showed a nonlinear increase in lasing intensity above the lasing threshold of 0.65 mJ/cm², and angle-resolved emission spectra measurements confirmed the lasing mode is from the Γ_2 band-edge state at $|\mathbf{k}_{\parallel}| = 0$ (**Figure S8**). To investigate the Γ_1 mode, we used IR140-DMSO (0.5 mM) as gain medium and pumped with a 800-nm fs-pulsed laser. Lasing at 865 nm with a measured input power threshold value of 0.45 mJ/cm² was achieved (**Figure 4e**). Hence, multipolar LSPs can achieve two high quality SLRs separated by 100s of nm using a honeycomb lattice with identical NPs at each lattice site and is the first structure to realize lasing at the spectral ends of the visible regime.³²

Conclusions

We investigated the formation of hierarchically hybridized SLRs in plasmonic honeycomb NP lattices. Near the NP surface, the interplay between the non-Bravais lattice symmetry and the LSP wavefunction basis results in anisotropic electric near-field distributions that result in asymmetric spatial distributions of stimulated emission rates. By engineering NP shape, material, and spacing, we achieved two distinct band-edge states separated by more than 300 nm from a single-lattice array. This magnitude represents a key advantage of hierarchically hybridized SLRs: the lattice geometry and LSP wavefunctions can be separately tuned to create multi-polar plasmonic lattices. We anticipate our findings will be critical in tuning near-field interactions between plasmonic NP lattices and emitters, for example in strong coupling and Bose-Einstein condensation. SLRs may also provide insight to photonic analogous of PT-symmetry and topological effects, especially since gain and loss in emitter-SLR systems can be exquisitely tailored.

Methods

Fabrication of Al and Au NP arrays

Arrays of Ag NPs on fused silica were fabricated with a soft nanofabrication process called PEEL.⁴⁶ Briefly, we generated periodic photoresist posts on Si wafers by solvent-assisted nanoscale embossing (SANE)⁴⁷ with controlled post size. The patterns were then transferred into free-standing Au nanohole films by depositing Cr film, removing PR posts, etching through Si nanoholes, depositing Au film, and lifting off Au film. Finally, we created NP arrays by thermal deposition through the hole-array mask on a transparent substrate and then used scotch tape to remove the Au hole mask. A 2-nm Cr layer was deposited in-between for better adhesion between Ag NPs and silica.

Lasing measurements

A drop of a 0.5 mM IR140-DMSO solution was placed on Ag NP arrays and capped with a coverslip. The completed sample was pumped at an incident angle of 45° using a mode-locked Ti:sapphire laser with a regenerative amplifier (800-nm wavelength, 1 kHz operation rate and 90 fs pulse width), and the circular pump spot size was ~800 μm in diameter. Lasing signals were collected normal to the sample surface and analyzed by a charge-coupled device (CCD) spectrometer. For angle-resolved emission measurements, we fixed the sample vertically at the centre of a rotational stage and collected emission signals within detection angle from 0° to 5° in 1° increments manually (with respect to the sample surface normal).

FDTD simulations

FDTD calculations with commercial software (FDTD solution, Lumerical Inc., Vancouver, Canada) were used to simulate the linear optical properties and lasing emission from Ag NP arrays. The optical constants of Ag were taken from Palik measurements (400–1000 nm).⁴⁸ A

uniform mesh size of 2 nm (x, y and z) was used to ensure the accuracy of electric and magnetic

field calculations within the metal NPs.

Simulation of Γ_1 lasing was performed by FDTD, where a four-level one-electron model was

integrated for modeling dye molecules. In the semi-quantum systems, we set the Ag NP size d =

110 nm and height h = 50 nm, dye concentration C = 0.5 mM, pump wavelength at $\lambda_a = 800$ nm

and dye emission at $\lambda_e = 850$ nm with bandwidth $\Delta \lambda_e = 120$ nm, close to experimental

conditions. The spontaneous emission rate (N_2/τ_{21}) and stimulated emission rate $(\frac{1}{\hbar w} E \frac{dP}{dt})$ were

analyzed to show their spatial correlation with the plasmonic hot spots with the amplitude of

pump power set to be 8×10^7 .

Supporting Information Available:

Hexagonal lattice characterization, Ag dimer spectra, Γ_1 lasing characterization (Ag NPs), Γ_1

lasing characterization (Al NPs), single Al NP scattering spectrum, Γ_2 lasing characterization (Al

NPs).

Author information

Corresponding author

*Email: g-schatz@northwestern.edu

*Email: todom@northwestern.edu

† These authors contributed equally to this work.

ORCID

Ran Li: 0000-0001-5606-3826

Marc R. Bourgeois: 0000-0002-9435-9051

Charles Cherqui: 0000-0003-2818-7973

15

Jun Guan: 0000-0001-8667-1611

Danqing Wang: 0000-0002-7369-1944

Jingtian Hu: 0000-0002-0528-6250

Richard D. Schaller: 0000-0001-9696-8830

George C. Schatz: 0000-0001-5837-4740

Teri W. Odom: 0000-0002-8490-292X

Acknowledgments

This work is supported by Vannevar Bush Faculty Fellowship from DOD under N00014-17-1-3023, NSF CHE-1760537, NSF DMR-1608258 and NSF DMR-1904385. This work used the Northwestern University Micro/Nano Fabrication Facility (NUFAB) and the EPIC and SPID facilities of Northwestern University's NUANCE Center, which is partially supported by Soft and Hybrid Nanotechnology Experimental (SHyNE) Resource (NSF ECCS-1542205), the Materials Research Science and Engineering Center (DMR-1720139), \ the MRSEC program (NSF DMR-1121262) at the Materials Research Center; the International Institute for Nanotechnology (IIN); the Keck Foundation; and the State of Illinois. This research was supported in part by the Quest high performance computing facility at Northwestern University, which is jointly supported by the Office of the Provost, the Office for Research, and Northwestern University Information Technology. Use of the Center for Nanoscale Materials, an Office of Science user facility, was supported by the U.S. Department of Energy, Office of Science, Office of Basic Energy Sciences, under Contract No. DE-AC02-06CH11357. CC would like to thank Professor Dave Dunlap from University of New Mexico for valuable discussions.

References

- 1. Aufray, B.; Kara, A.; Vizzini, S.; Oughaddou, H.; Leandri, C.; Ealet, B.; Le Lay, G. Graphene-like silicon nanoribbons on Ag (110): A possible formation of silicene. *Appl. Phys. Lett.* **2010**, 96, 183102.
- 2. Durgun, E.; Tongay, S.; Ciraci, S., Silicon and III-V compound nanotubes: structural and electronic properties. *Phys. Rev. B* **2005**, 72, 075420.
- 3. Ataca, C.; Sahin, H.; Ciraci, S., Stable, single-layer MX2 transition-metal oxides and dichalcogenides in a honeycomb-like structure. *J. Phys. Chem. C* **2012**, 116, 8983-8999.
- 4. Kane, C. L.; Mele, E. J., Quantum spin Hall effect in graphene. *Phys. Rev. Lett.* **2005**, 95,226801.
- 5. Kelly, K. L.; Coronado, E.; Zhao, L. L.; Schatz, G. C., The optical properties of metal nanoparticles: The influence of size, shape, and dielectric environment. *J. Phys. Chem. B* **2003**, 107, 668-677.
- 6. Haynes, C. L.; Mcfarland, A. D.; Zhao, L.; Duyne, R. P. V.; Schatz, G. C.; Gunnarsson, L.; Prikulis, J.; Kasemo, B.; Ka, M., Nanoparticle Optics: The Importance of Radiative Dipole Coupling in Two-Dimensional. *J. Phys. Chem. B* **2003**, 7337-7342.
- 7. Cahangirov, S.; Topsakal, M.; Aktürk, E.; Şahin, H.; Ciraci, S., Two-and one-dimensional honeycomb structures of silicon and germanium. *Phys. Rev. Lett.* **2009**, 102, 236804.
- 8. Li, T.; Galli, G., Electronic properties of MoS2 nanoparticles. *J. Phys. Chem. C* **2007**, 111, 16192-16196.
- 9. Polini, M.; Guinea, F.; Lewenstein, M.; Manoharan, H. C.; Pellegrini, V., Artificial honeycomb lattices for electrons, atoms and photons. *Nat. Nanotechnol.* **2013**, 8, 625-633.
- 10. Weick, G.; Woollacott, C.; Barnes, W. L.; Hess, O.; Mariani, E., Dirac-like plasmons in honeycomb lattices of metallic nanoparticles. *Phys. Rev. Lett.* **2013**, 110, 1-6.
- 11. Odom, T. W.; Gao, H.; McMahon, J. M.; Henzie, J.; Schatz, G. C., Plasmonic superlattices: Hierarchical subwavelength hole arrays. *Chem. Phys. Lett.* **2009**, 483, 187-192.
- 12. Wang, D.; Yang, A.; Hryn, A. J.; Schatz, G. C.; Odom, T. W., Superlattice plasmons in hierarchical Au nanoparticle arrays. *ACS Photonics* **2015**, 2, 1789-1794.
- 13. Ramezani, M.; Halpin, A.; Feist, J.; Van Hoof, N.; Fernández-Domínguez, A. I.; Garcia-Vidal, F. J.; Gómez Rivas, J., Dispersion Anisotropy of Plasmon–Exciton–Polaritons in Lattices of Metallic Nanoparticles. *ACS Photonics* **2017**, *5*, 233-239.
- 14. Murai, S.; Fujita, K.; Daido, Y.; Yasuhara, R.; Kamakura, R.; Tanaka, K., Plasmonic arrays of titanium nitride nanoparticles fabricated from epitaxial thin films. *Opt. Express* **2016**, 24, 1143-1153.
- 15. Guo, R.; Hakala, T. K.; Törmä, P., Geometry dependence of surface lattice resonances in plasmonic nanoparticle arrays. *Phys. Rev. B* **2017**, 95, 155423.
- 16. Lin, C.-H.; Chen, H.-L.; Chao, W.-C.; Hsieh, C.-I.; Chang, W.-H., Optical characterization of two-dimensional photonic crystals based on spectroscopic ellipsometry with rigorous coupled-wave analysis. *Microelectron. Eng.* **2006**, 83, 1798-1804.
- 17. Wagner, R.; Cichos, F., Fast measurement of photonic stop bands by back focal plane imaging. *Phys. Rev. B* **2013**, 87, 165438.
- 18. Robertson, W.; Arjavalingam, G.; Meade, R.; Brommer, K.; Rappe, A. M.; Joannopoulos, J., Measurement of photonic band structure in a two-dimensional periodic dielectric array. *Phys. Rev. Lett.* **1992**, 68, 2023-2026.

- 19. Labilloy, D.; Benisty, H.; Weisbuch, C.; Krauss, T.; De La Rue, R.; Bardinal, V.; Houdré, R.; Oesterle, U.; Cassagne, D.; Jouanin, C., Quantitative measurement of transmission, reflection, and diffraction of two-dimensional photonic band gap structures at near-infrared wavelengths. *Phys. Rev. Lett.* **1997**, 79, 4147-4150.
- 20. Humphrey, A. D.; Barnes, W. L., Plasmonic surface lattice resonances on arrays of different lattice symmetry. *Phys. Rev. B* **2014**, 90, 075404.
- 21. Guo, R.; Nečada, M.; Hakala, T. K.; Väkeväinen, A. I.; Törmä, P., Lasing at K Points of a Honeycomb Plasmonic Lattice. *Phys. Rev. Lett.* **2019**, 122, 013901.
- 22. Evlyukhin, A. B.; Reinhardt, C.; Zywietz, U.; Chichkov, B. N., Collective resonances in metal nanoparticle arrays with dipole-quadrupole interactions. *Phys. Rev. B* **2012**, 85, 245411.
- 23. Wang, L.; Zhang, R. Y.; Xiao, M.; Han, D.; Chan, C. T.; Wen, W., The existence of topological edge states in honeycomb plasmonic lattices. *New J. Phys.* **2016**, 18, 103029.
- 24. Wang, D.; Bourgeois, M. R.; Lee, W.-K.; Li, R.; Trivedi, D.; Knudson, M. P.; Wang, W.; Schatz, G. C.; Odom, T. W., Stretchable Nanolasing from Hybrid Quadrupole Plasmons. *Nano Lett.* **2018**, 18, 4549-4555.
- 25. Lu, L.; Joannopoulos, J. D.; Soljačić, M., Topological photonics. *Nat. Photon.* **2014,** 8, 821-829.
- 26. Noh, J.; Benalcazar, W. A.; Huang, S.; Collins, M. J.; Chen, K. P.; Hughes, T. L.; Rechtsman, M. C., Topological protection of photonic mid-gap defect modes. *Nat. Photon.* **2018**, 12, 408-415.
- 27. Downing, C. A.; Weick, G., Topological collective plasmons in bipartite chains of metallic nanoparticles. *Phys. Rev. B* **2017**, 95, 125426.
- 28. Pocock, S.; Xiao, X.; Huidobro, P. A.; Giannini, V., The topological plasmonic chain with retardation and radiative effects. *ACS Photonics* **2018**, 5, 2271-2279.
- 29. Zou, S.; Janel, N.; Schatz, G. C., Silver nanoparticle array structures that produce remarkably narrow plasmon lineshapes. *J. Chem. Phys.* **2004**, 120, 10871-10875.
- 30. Wu, L.-H.; Hu, X., Scheme for achieving a topological photonic crystal by using dielectric material. *Phys. Rev. Lett.* **2015**, 114, 223901.
- 31. Henzie, J.; Lee, M. H.; Odom, T. W., Multiscale patterning of plasmonic metamaterials. *Nat. Nanotechnol.* **2007**, 2, 549.
- 32. Wang, D.; Yang, A.; Wang, W.; Hua, Y.; Schaller, R. D.; Schatz, G. C.; Odom, T. W., Band-edge engineering for controlled multi-modal nanolasing in plasmonic superlattices. *Nat. Nanotechnol.* **2017**, 12, 889.
- 33. Hohenester, U.; Trugler, A., MNPBEM A Matlab toolbox for the simulation of plasmonic nanoparticles. *Comput. Phys. Commun.* **2012**, 183, 370-381.
- 34. Sherry, L. J.; Chang, S. H.; Schatz, G. C.; Van Duyne, R. P.; Wiley, B. J.; Xia, Y. N. Localized surface plasmon resonance spectroscopy of single silver nanocubes. *Nano Lett.* **2005**, 5, 2034-2038.
- 35. Cherqui, C.; Li, G. L.; Busche, J. A.; Quillin, S. C.; Camden, J. P.; Masiello, D. J., Multipolar Nanocube Plasmon Mode-Mixing in Finite Substrates. *J. Phys. Chem. Lett.* **2018**, 9, 504-512.
- 36. Zhou, W.; Dridi, M.; Suh, J. Y.; Kim, C. H.; Co, D. T.; Wasielewski, M. R.; Schatz, G. C.; Odom, T. W., Lasing action in strongly coupled plasmonic nanocavity arrays. *Nat. Nano.* **2013**, 8, 506-511.

- 37. Knudson, M. P.; Li, R.; Wang, D.; Wang, W.; Schaller, R. D.; Odom, T. W., Polarization-Dependent Lasing Behavior from Low-Symmetry Nanocavity Arrays. *ACS Nano* **2019**, 13, 7435-7441.
- 38. Willner, A. E.; Byer, R. L.; Chang-Hasnain, C. J.; Forrest, S. R.; Kressel, H.; Kogelnik, H.; Tearney, G. J.; Townes, C. H.; Zervas, M. N., Optics and photonics: Key enabling technologies. *Proc. IEEE.* **2012**, 100, 1604-1643.
- 39. Wang, W.; Watkins, N.; Yang, A.; Schaller, R. D.; Schatz, G. C.; Odom, T. W., Ultrafast Dynamics of Lattice Plasmon Lasers. *J. Phys. Chem. Lett.* **2019**, 10, 3301-3306.
- 40. Li, R.; Wang, D.; Guan, J.; Wang, W.; Ao, X.; Schatz, G. C.; Schaller, R.; Odom, T. W., Plasmon nanolasing with aluminum nanoparticle arrays. *JOSA B* **2019**, 36, E104-E111.
- 41. Yang, A.; Hryn, A. J.; Bourgeois, M. R.; Lee, W.-K.; Hu, J.; Schatz, G. C.; Odom, T. W., Programmable and reversible plasmon mode engineering. *Proc. Natl. Acad. Sci.* **2016**, 113, 14201-14206.
- 42. Vasa, P.; Wang, W.; Pomraenke, R.; Lammers, M.; Maiuri, M.; Manzoni, C.; Cerullo, G.; Lienau, C., Real-time observation of ultrafast Rabi oscillations between excitons and plasmons in metal nanostructures with J-aggregates. *Nat. Photon.* **2013**, 7, 128-132.
- 43. Shi, L.; Hakala, T. K.; Rekola, H. T.; Martikainen, J. P.; Moerland, R. J.; Torma, P., Spatial Coherence Properties of Organic Molecules Coupled to Plasmonic Surface Lattice. Resonances in the Weak and Strong Coupling Regimes. *Phys. Rev. Lett.* **2014**, 112, 153002.
- 44. Liu, W. J.; Lee, B.; Naylor, C. H.; Ee, H. S.; Park, J.; Johnson, A. T. C.; Agarwal, R., Strong Exciton-Plasmon Coupling in MoS2 Coupled with Plasmonic Lattice. *Nano Lett.* **2016**, 16, 1262-1269.
- 45. Hakala, T. K.; Moilanen, A. J.; Vakevainen, A. I.; Guo, R.; Martikainen, J. P.; Daskalakis, K. S.; Rekola, H. T.; Julku, A.; Torma, P., Bose-Einstein condensation in a plasmonic lattice. *Nat. Phys.* **2018**, 14, 739-744.
- 46. Henzie, J.; Barton, J. E.; Stender, C. L.; Odom, T. W., Large-area nanoscale patterning: chemistry meets fabrication. *Acc. Chem. Res.* **2006**, 39, 249-257.
- 47. Lee, M. H.; Huntington, M. D.; Zhou, W.; Yang, J.-C.; Odom, T. W., Programmable soft lithography: solvent-assisted nanoscale embossing. *Nano Lett.* **2010**, 11, 311-315.
- 48. Palik, E. D., Handbook of optical constants of solids. Academic press: 1998.

Table of Contents

